Slow cooling during crystallisation of barred olivine chondrules

François Faure, Marion Auxerre, Valentin Casola

Slow cooling during crystallisation of barred olivine chondrules

François Faure[1]*, Marion Auxerre[1], Valentin Casola[1]

[1]Université de Lorraine, CNRS, CRPG, UMR 7358, 15 rue Notre Dame des Pauvres F-54501 Vandoeuvre-lès-Nancy France.

* Corresponding author: francois.faure@univ-lorraine.fr

ABSTRACT

Barred olivine (BO) chondrules are small ferromagnesian silicate igneous droplets with unique dendritic textures that are considered to have formed in the early solar system during one or more brief high-temperature episodes, followed by rapid cooling in a gas. Rapid cooling rates of 100–7200 °C/h during chondrule formation have been proposed based on experiments attempting to reproduce BO crystal textures. However, the BO texture has never truly been reproduced under such rapid cooling conditions. Here, we experimentally show that true BO textures can be produced either after rapid cooling (>50 °C/h) following by reheating step or by cooling rates slower than 10 °C/h. Regardless of the thermal history considered, the chemical compositions of glass inclusions trapped within olivines of BO chondrules imply a final slow cooling rate one to two orders of magnitude below previous estimates. Such slow cooling rates are consistent with those estimated for plagioclase-bearing porphyritic chondrules and magmatic type-B Ca-Al-rich inclusions, suggesting that slow cooling rates are common to all similar chondritic objects.

Keywords: chondrule, olivine, dendrite, crystal growth, glass inclusion.

1. Introduction

Chondrules are the principal constituents of the least altered chondritic meteorites; they are small ferromagnesian silicate igneous droplets considered to have formed in the early solar system during one or more brief high-temperature episodes followed by rapid cooling in a gas (Jones et al., 2000; Rubin, 2000 and references therein). A key parameter in chondrule formation models is the cooling rate, which is generally constrained by experimental results (Connolly and Desch, 2004; Desch et al., 2012; Jones et al., 2018) and varies greatly among chondrule types. Porphyritic chondrules were not initially completely molten and their resultant textures were essentially controlled by the presence of relict crystals or crystal nuclei in the melt (Lofgren, 1989; Lofgren and Russell, 1986). Therefore, cooling rates spanning 0.5–1000 °C/h are generally proposed to replicate porphyritic textures (see Jones et al., 2018 for a recent compilation). Only plagioclase-bearing porphyritic chondrules seem to impose very slow cooling rates (1 °C/h) at the end of crystallisation (Wick and Jones, 2012). Among non-porphyritic chondrules, it is well established that barred olivine (BO) chondrules were initially fully molten (Hewins and Radomsky, 1990); BO crystallisation during cooling did not require triggering by collisions between molten chondrules and mineral dust, as it was generally proposed to explain radial non-porphyritic chondrules (Connolly and Hewins, 1995), even if radial pyroxene textures can also be obtained by rapid cooling after an initial step of total melting (Hewins et al., 1981). Thus, only BO chondrules can be used without ambiguity to reliably constrain non-porphyritic chondrule cooling rates.

BO chondrules are droplet shaped, contain parallel bars of olivine set in glass, and are typically rimmed by an olivine shell (Fig. 1; Weisberg, 1987). Olivine bars and rim are optically continuous and therefore correspond to a single crystal. In three dimensions, the bars correspond to platy crystals that are attached to the olivine shell in a comb-like texture (Gooding and Keil, 1981; Noguchi, 2002; Tsuchiyama et al., 2000). This definition

corresponds to ‘classic’ BO chondrules; ‘multiple’ BO chondrules comprise several grouplets of parallel bars/plates, with each grouplet corresponding to an individual crystal (Weisberg, 1987). Although these parallel bars/plates display smooth surfaces, this peculiar texture has generally been termed a ‘dendritic’ bar or plate texture (Lofgren and Lanier, 1990; Tsuchiyama et al., 2004); only recently have high-resolution cathodoluminescence images confirmed the presence of true dendritic textures in the cores of these olivine bars (Libourel and Portail, 2018). Nonetheless, previous dynamic crystallisation experiments attempting to reproduce BO textures at 1 atm have explored a vast range of rapid cooling rates spanning 100–7200 °C/h (Lofgren, 1989; Lofgren and Lanier, 1990; Radomsky and Hewins, 1990; Connolly and Hewins, 1991; Kennedy et al., 1993; Tsuchiyama et al., 2000). These experiments reproduced well the sets of parallel olivine dendrites, but, with rare exceptions, failed to reproduce the characteristic external rims of BO chondrules (Lofgren and Lanier, 1990; Radomsky and Hewins, 1990).

Experiments employing levitation systems to avoid heterogeneous nucleation on the surface of the sample holder have produced bars and rims at even faster cooling rates of 36×10^4–10^5 °C/h (Tsukamoto et al., 2001). However, these experiments used pure forsterite composition, and the crystal growth rates obtained are almost one order of magnitude faster than those measured in more complex compositional systems (Jambon et al., 1992). In contrast, Nagahara (1996) reproduced the BO texture isothermally (i.e., without cooling) under vacuum to determine evaporation kinetics in the simple MgO-SiO_2 system. Tsuchiyama et al. (2004) also reproduced the BO texture (rim and bars) under vacuum from a complex analogue chondrule composition, but at relatively rapid cooling rates (500–1000 °C/h). Therefore, excluding the isothermal experiments of Nagahara (1996) because the composition was probably too simple to allow growth controlled by chemical diffusion, all previous experiments (under vacuum, at 1 atm, or using levitation) suggest that the BO texture results

from rapid cooling rates (10^2–10^6 °C/h). However, Tsuchiyama et al. (2004) noted that *true* BO textures have never been reproduced because experimental olivines always display a marked dendritic morphology whereas bars in natural BO chondrules are generally smooth. Moreover, glass inclusions in natural olivine bars display round or ovoid shapes (Varela et al., 2006), not the 'negative' dendritic crystal shapes produced in experiments. Therefore, it was suggested that natural BO textures may result from rapid cooling following by annealing at high temperature (Tsuchiyama et al., 2004). However, it has never been considered that BO textures were simply produced at slow cooling rates. Therefore, we here experimentally tested both a large range of cooling rates (5–1000 °C/h) and the annealing hypothesis, and our results show that BO chondrules formed under slow cooling rates.

2. Methods

The chemical compositions of natural BO chondrules vary greatly, suggesting that composition is not the principal parameter controlling this texture. Therefore, we used a simplified chondritic composition and added Al, Ca, and Fe^{3+} to diminish the MgO content and thus the liquidus temperature, as proposed by Dehart and Lofgren (1996). The Al_2O_3/CaO ratio in our composition (1.42) is between that used to simulate CI-like materials (1.55) by Cohen et al. (2004) and that proposed by Anders and Grevesse (1989) for CI chondrites (1.26).

The starting glass material was prepared from a mixture of reagent-grade oxides (38 wt.% SiO_2, 10 wt.% Al_2O_3, 7 wt.% CaO, 18 wt.% MgO, 27 wt.% Fe_2O_3), melted in a platinum crucible at 1650 °C (about 200 °C above the liquidus temperature in oxidising conditions, T_{liq} = 1440 °C, as determined by isothermal experiments) for 1 h in air, and quenched in water. The glass obtained was then ground to a powder in an agate mortar and pestle, loaded into a carbon crucible within an alumina crucible, and hung near the end of a

ceramic rod in the hot spot of a Nabertherm vertical furnace. The samples were introduced directly into the preheated furnace, and the air volume inside the alumina tube of the furnace was then evacuated by a primary pump at the bottom of the furnace. Pressure was monitored using a gauge positioned in the upper part of the alumina tube. Experiments were conducted under vacuum (P < 10 Pa) to allow evaporation of the moderately volatile species Fe, Mg, and Si. The carbon crucible was used to form nearly spherical samples by exploiting the poor wetting between silicate liquids and graphite (Tsuchiyama et al., 2004; Faure et al., 2006).

We used three thermal protocols in this study.

The first corresponded to isothermal experiments to ensure that all dynamic crystallisation experiments (second protocol, below) began well above the liquidus temperature. Three sets of isothermal experiments were performed at 1450 °C (i.e., 10 °C above the oxidising liquidus temperature previously determined by isothermal experiments in air), 1500 °C, and 1600 °C for various heating durations. However, it is difficult to precisely determine the liquidus temperature in our experiments for two reasons. First, under vacuum, the chemical composition of the starting liquid changed via evaporation during the experiments. Second, the oxidation state of iron in the charge also changed during the experiments: initially in its oxidised state (Fe^{3+}), heating the liquid in a carbon crucible reduced iron to Fe^{0}.

The second protocol corresponded to dynamic crystallisation experiments. These experiments began with isothermal heating (2 h) at 1600 °C (at least 100 °C above the liquidus temperature) followed by cooling to 1200–1210 °C at rates of 5–1000 °C/h before quenching in air (Table 1). Four experiments (25-N267 and 26-N268, cooled at 500 °C/h, and 32-N274 and 33-N273, cooled at 50 °C/h) were quenched at higher temperatures of 1400 and 1300 °C, respectively. Moreover, experiment 27-N260 was held isothermally at 1200 °C for 2 h before quenching, and experiment 28-N263 was held at 1200 °C for 4 h before a second

stage of cooling at 300 °C/h down to 900 °C, at which temperature the charge was held isothermally for 62 h before the air quench.

The third protocol was similar to the second, but at the end of the cooling step, the charges were reheated to 1400 or 1500 °C for various durations before quenching in air (Table 2).

At the end of all experiments, the charges were quenched in air by rapidly removing the ceramic rod holding the sample crucible. Therefore, regardless of the thermal protocol, the quench rate was not very rapid and allowed the formation of quench crystals.

After quenching, the charges were mounted in epoxy and prepared as polished sections. Samples were examined using a scanning electron microscope (JEOL 6510) equipped with a Bruker AXS Xflash detector "Quantax" operating in energy dispersive mode (EDS) at the CRPG. Chemical analyses were performed with an accelerating voltage and beam current of 15 kV and 0.25 nA, respectively, in analytical mode (EDS).

3. Results

Experimental conditions and results are detailed in Tables 1 and 2. Chemical composition of olivines formed during dynamic crystallization experiments are given in supplementary Table S1.

3.1. Isothermal evaporation experiments

Three temperatures were investigated to estimate the liquidus temperature of the starting composition as a function of the evaporation duration and the changing iron oxidation state. It is important to note that, although experiments were performed isothermally, equilibrium was never achieved because the system was open.

152 *3.1.1. Experiments at 1450 °C*

153 Experiments at this temperature had durations of 5 min to 16 h. All experiments
154 displayed polyhedral olivines with skeletal or dendritic overgrowths, but dendritic olivine
155 rods appeared in experiments longer than 15 min (Supplementary Fig. S1a) and became
156 increasingly numerous at longer durations. These rods comprised units displaying H or dove
157 shapes according to the dendritic olivine nomenclature of Donaldson (1976) and Faure et al.
158 (2003a, 2003b). Rods occurred as either single rods randomly distributed throughout the
159 charge or grouplets of parallel bars resembling the BO texture (Fig. S1b). However, the
160 persistence of polyhedral and skeletal crystals, particularly along the borders of the charges,
161 implies that the liquidus temperature was never attained in these experiments, even at the
162 longest duration.

163

164 *3.1.2. Experiments at 1500 °C*

165 Isothermal experiments at 1500 °C had durations of 5 min to 7 h. These experiments
166 can be subdivided into three groups as a function of experimental duration.

167 The first group includes only the shortest duration experiment (5 min). This charge
168 was texturally similar to charges heated at 1450 °C; polyhedral and skeletal olivines were
169 distributed around the border, and the centre of the charge was occupied by dendritic olivine
170 rods.

171 The second group includes charges heated between 15 min and 3 h. These charges
172 (except that heated for 1 h) displayed only dendritic olivine crystals oriented randomly. The
173 charge heated for 1 h contained spinel crystals instead of dendritic olivines. It is unclear what
174 caused this difference in mineralogy, but our best explanation is that it resulted from a slight
175 variation in the evaporation rate, which increased the Al content in the residual liquid, making
176 spinel the stable phase instead of olivine. This seems consistent with the fact that the third

group of experiments at this temperature, charges heated for long durations of 5 and 7 h, contained aggregates of Al-Ca-rich crystals within an Al-Ca-rich mesostasis; in these experiments Mg and Fe had totally disappeared, and only trace amounts of Si were analysed by EDS.

3.1.3. Experiments at 1600 °C

All samples obtained after isothermal evaporation at 1600 °C (Table 1) displayed only rod-shaped dendritic olivine crystals embedded in a glassy mesostasis. Rods were either randomly distributed in the charge or comprised sets of perfectly parallel rods. Olivine crystals displayed the same dendritic morphology and size range (rod widths of 10–50 μm, depending on sectioning) regardless of heating duration (5 min to 5 h). This result suggests that these dendritic crystals were produced during the quench, in turn implying that the charges were totally melted during the isothermal step. However, it is important to note that olivine rims never formed in charges that experienced only an isothermal heating step.

3.2. Cooling experiments

After isothermally heating charges at 1600 °C for 2 h to ensure that they were initially totally molten, we tested a large range of cooling rates from 5 to 1000 °C/h. To a first approximation, all charges showed textures resembling the BO texture (Fig. 2). All experiments quenched at ≤1300 °C showed one to five sets of parallel olivine bars, regardless of the cooling rate (Table 1); charges quenched at 1400 °C contained more numerous crystallographically distinct crystals (48–62 sets of bars), as observed in samples isothermally heated at 1600 °C. The thickness of bars in a given crystal (i.e., set of parallel bars) was usually variable (Fig. 2c–f) and mostly depended on sectioning effects rather than the cooling rate. Rods either spanned the entire charge or were developed only on one side. When two

rods grew on opposite sides of the charge, but not rigorously face-to-face, the junction between them was distorted and misoriented. Then, rods displayed waves and were commonly slightly misoriented with respect to the main direction of elongation of the set. In this case, we refer to the shape of rods as "corrugated". Rods were continuous or variably segmented regardless of the cooling rate (Fig. 2). In all dynamic crystallisation experiments (i.e., regardless of cooling rate), we observed discontinuous areas of olivine rimming the borders of the charges, but none had rims around the entire circumference of the charge. There is no clear relation between rim thickness and cooling rate; we thus attribute variations in rim thickness to sectioning effects.

Although all dynamic crystallisation experiments broadly resembled the BO texture, two groups can be defined in detail: rapid (50–1000 °C/h) and slow cooling experiments (5 and 10 °C/h).

In rapid cooling experiments (>50 °C/h), olivine rods showed the same dendritic shapes as those observed in isothermal experiments. H- or dove-shaped units were very well formed in the charges that were cooled the fastest (500 and 1000 °C/h). The dove shape was more difficult to recognize in charges cooled at 50–250 °C/h; only the sides of the doves (wings) were consistently visible (Fig. 3a, b). In contrast, H- or dove-shaped units were not present in slowly cooled charges (5 and 10 °C/h); in those cases, rods or corrugated segmented rods had smooth, flat surfaces. Similarly, glass inclusions within rapidly cooled rods (500 or 1000 °C/h) showed characteristic ‘negative’ crystal (dove) shapes, whereas, with decreasing cooling rate (≤250 °C/h), the limiting faces of inclusions became more rounded. At cooling rates ≤10 °C/h, glass inclusions systematically had round or ovoid shapes.

The external rims of the charges also showed morphological variations as a function of cooling rate (Fig. 4). Rims formed during rapid cooling experiments displayed dendritic shapes, whereas rim became more rounded and undulous at slower cooling rates. This

transition seems to have occured around 50 °C/h; at that cooling rate, rods attached to the rim had smooth, wavy shapes, whereas rods well within the charge were always dendritic. At ≤10 °C/h, both rims and rods had smooth, wavy shapes and contained rounded glass inclusions (Fig. 4d, e). We note that pure euhedral spinel crystals ($MgAl_2O_4$) were present inside the charge that cooled at the slowest rate, i.e., the charge that spent the most time at high temperature and thus endured the most protracted evaporation (Fig. 4f).

3.3. Charges cooled, then isothermally held before quenching

We performed two experiments to estimate the effect of an isothermal step before quenching (Table 1). After cooling by 500 °C/h, these charges were held isothermally at 1200 °C for 2 h and then quenched (27-N260) or held at 1200 °C for 4 h, cooled to 900 °C by 300 °C/h and held isothermally for 62 h, and finally quenched (28-N263). No significant differences were apparent between charges held isothermally at high temperature and those that only experienced cooling at 500 °C/h (Figs. 2b, 5). However, in detail, the charge held isothermally for 2 h showed incipient textural ripening, although the wings of the dove's units were still present (Fig. 5b). In contrast, the charge held isothermally for 4 h before a second cooling step displayed relatively smooth bars, although glass inclusions still had 'negative' dove shapes (Fig. 5d).

3.4. Cooling and reheating experiments

We performed five experiments initially cooled to 1200 °C then reheated to 1400 or 1500 °C. Of these, four were initially cooled by 500 °C/h before reheating (three to 1400 °C and one to 1500 °C); the fifth was cooled by 50 °C/h before reheating to 1400 °C (Table 2).

3.4.1. Experiments reheated to 1400 °C

252 The three experiments cooled at 500 °C/h then reheated to 1400 °C no longer showed
253 rods comprising dove units, but instead contained rods with smooth surfaces (Fig. 6a–f). Rods
254 were either continuous or formed from smaller segments. Rod segmentation increased with
255 increasing time spent at the reheated temperature, consistent with textural ripening (although
256 sectioning effects cannot be ruled out).

257 The first experiment was directly quenched after reheating to 1400 °C. That charge
258 displayed, to a first approximation, a texture that best matches the "classic" BO chondrule
259 texture because it contained both mostly parallel bars and a prominent rim. However, some
260 bars showed slight misorientations; these may represent several distinct olivine crystals.
261 Moreover, the rim is discontinuous and slightly offset from the border of the charge. These
262 two observations could represent an experimental artifact. Indeed, on the one hand,
263 Tsuchiyama et al. (2004) showed that contact with the carbon capsule precludes the formation
264 of a continuous rim. On the other hand, the offset of the border of the charge is probably due
265 to the air quench when the sample was rapidly removed from the vertical furnace, which
266 would be consistent with the small dendrites that grew in the free space between the olivine
267 rim and the border of the charge. Similarly, both experiments reheated and held isothermally
268 for 3 and 12.5 h showed numerous small dendritic olivine bars and dendritic overgrowths on
269 segments, suggesting that the dendrites resulted from the quench. Moreover, this quench
270 texture is consistent with the high MgO content of the liquid, which is due to reheating to
271 1400 °C. After ≥3 h of reheating, inclusions within olivine bars were ovoid and resemble
272 natural glass inclusions (Fig. 6d).

273 The experiment initially cooled by 50 °C/h before reheating to 1400 °C and held
274 isothermally for 11 h before quenching showed bars that were more or less segmented
275 depending on the section viewed. The larger segments were euhedral, with well-developed
276 external faces, even if containing a large central hole recalling their former skeletal shape, i.e.,

hopper crystals (Fig. 6g). Most glass inclusions were ovoid in shape. Moreover, numerous overgrowths and dendritic olivines (quench crystals) were superimposed on the initial BO texture.

3.4.2. Experiment reheated to 1500 °C

The experiment reheated to 1500 °C showed numerous dendritic olivine crystals resembling those produced during the quench of 2h isothermal experiments at 1500 or 1600 °C (Fig. S2). This observation suggests that these dendritic crystals resulted from the quench and do not correspond to the ripening of crystals formed during the initial cooling step. Therefore, reheating to 1500 °C must have melted all crystalline phases formed during the initial cooling step, and the charge was totally liquid before the quench.

4. Discussion

Numerous experiments over the past few decades have apparently reproduced barred olivines as observed in chondrules. However, no clear consensus exists on the thermal conditions necessary to produce barred olivines. This results from the fact that multiple thermal parameters must be considered (degree of superheating, degree of undercooling, cooling rate), and because even the definition of a barred olivine chondrule varies among researchers. Therefore, we here first discuss the definition a barred olivine chondrule before exploring the thermal parameters required to truly reproduce of this peculiar texture.

4.1. Definition of barred olivine chondrules

As indicated by their name, barred olivines constitute bars that are parallel when belonging to the same crystal. Therefore, bars oriented in several directions suggest the presence of several crystals, unless a twinning law can explain the misorientation. However,

only a few crystals are observed in natural BO chondrules, varying from one in "classic" BO chondrules to eight in "multiple grouplet" BO chondrules. Another criterion defining barred olivines is the presence of an external olivine rim connected to the bars. Furthermore, the shape of the bars must be considered. In natural BO chondrules, bars have smooth or slightly curved faces, and never complex faceted arrangements that would correspond to a true dendritic morphology. Similarly, glass inclusions within olivine bars display rounded or ovoid shapes, not ‘negative’ dendritic crystal shapes.

Based on these five criteria (few crystals, sets of parallel bars, the presence of an olivine rim, smooth bar faces, round glass inclusions), we now discuss which thermal protocol best reproduces the BO texture.

4.1.1. Thermal conditions producing few crystals

In contrast to porphyritic chondrules, BO chondrules characteristically contain only a few crystals. This major difference in chondrule texture has been explained by the extent of melting of chondrule precursors (Lofgren, 1989; Connolly et al., 1998; Tsuchiyama et al., 2004). Partial melting promotes heterogeneous nucleation on relict crystals or nuclei that survived the melting event; in this case, crystal growth begins immediately upon cooling, forming porphyritic chondrules comprising numerous polyhedral crystals. In contrast, crystallisation following complete initial melting requires nucleation, implying that an energetic barrier must be overcome (Kirkpatrick, 1983). A recent experimental study has shown that the number of crystals produced experimentally varies by one to two orders of magnitude depending on whether the charge was initially completely or only partially melted (Auxerre et al., in press). Our results here confirm that charges heated above their liquidus temperature (superliquidus experiments) form few (1–5) crystals, regardless of the cooling rate considered (5–1000 °C/h). Moreover, even if the liquidus temperature was not well

constrained in our open-system experiments (due to evaporation and variation of the oxidation state of iron), our isothermal experiments longer than 15 minutes at 1500 °C and dynamic crystallisation experiments reheated to 1500 °C demonstrate that olivine crystals cannot survive at this temperature (Fig. S2). Indeed, these different experimental charges showed similar dendritic quench textures comprising numerous crystals (40–80), i.e., at least an order of magnitude more crystals than in superliquidus cooling experiments. Therefore, the liquidus temperature in our experiments was below 1500 °C, but must have been above 1450 °C according to isothermal experiments. We therefore assume that the liquidus temperature was near 1500 °C and that the degree of superheating (+ΔT) at the beginning of dynamic crystallisation experiments was around of 100 °C. Such a degree of superheating is sufficient to ensure initial total melting but low enough that nucleation should not be suppressed. Indeed, nucleation is totally suppressed at degrees of superheating exceeding 400 °C (Connolly et al., 1998), although the duration of heating also effects nucleation (First et al., 2020). Therefore, our experiments confirm that the BO texture requires that chondrules were initially completely molten (Lofgren, 1989; Connolly et al., 1998; Tsuchiyama et al., 2004).

4.1.2. Thermal conditions promoting the crystallisation of dendritic olivines

It is well known that dendritic morphologies result from crystallisation at a high degree of undercooling. Such degrees of undercooling can be induced by delayed nucleation, which is promoted by initial superheating, as suffered by natural BO chondrules (see section 4.1.1). In our experiments, because the solidification process was not observed in situ, we cannot directly measure the timing and temperature of nucleation. However, by quenching two series of experiments (cooling rates of 500 and 50 °C/h) at three different temperatures, we showed that charges were always completely liquid at 1400 °C. In contrast, at 1300 °C, olivine crystals corresponded to the BO texture, not a dendritic quench texture, suggesting

that the degree of undercooling due to delayed nucleation was around 100 °C. However, this value is not well constrained because we did not quench any experiments at temperatures between 1300 and 1400 °C, and because the liquidus temperature evolved in our open-system experiments. Therefore, determining the degree of undercooling in our experiments precisely is beyond the scope of this study. Nevertheless, we estimate the degree of undercooling was around 100 °C, regardless of the cooling rate tested, which is consistent with the occurrence of dendritic crystallisation in the charges.

4.1.3. Thermal conditions promoting the formation of parallel olivine bars

Numerous previous experiments have reproduced olivines displaying parallel dendritic bars over a large range of cooling rates (Donaldson, 1976; Tsuchiyama et al., 1980; Lofgren, 1989; Lofgren and Lanier, 1990; Radomsky and Hewins, 1990; Connolly and Hewins, 1991; Kennedy et al., 1993; Connolly et al., 1998; Faure et al., 2003a, 2006). This observation is consistent with our results that parallel olivine bars are observed at any cooling rate between 5 and 1000 °C/h. Even charges that were only isothermally melted well above their liquidus temperature produced parallel bars during the quench, although this result is clearly an experimental artifact because the air quench is not fast enough to chill MgO-rich liquid into glass. Even if it is not possible to constrain the cooling rate during quenching precisely, the quench rate is necessarily faster than all other cooling rates explored in our controlled cooling experiments. Therefore, the presence of parallel bars does not seem to be a reliable criterion for estimating the cooling rate of BO chondrules.

4.1.4. Thermal conditions producing an olivine rim around the chondrule

Reproducing the external rims around BO chondrules has long been an experimental difficulty (Miura et al. 2011). As noted by Tsuchiyama et al. (2004), only two prior

377 experiments reproduced this peculiar texture with conventional experimental techniques (i.e.,
378 in 1-atm furnaces), although the experimental conditions that produced the rims were not
379 clear. In contrast, experiments performed under vacuum produced olivine rims (Nagahara,
380 1996; Tsuchiyama et al., 2004). Tsuchiyama et al. (2004) succeeded in reproducing both
381 olivine rims and parallel bars over a large range of cooling rates between 500 and 1200 °C/h
382 under vacuum. However, the olivine rims they produced displayed dendritic shapes not
383 observed in natural BO chondrules. This result is consistent with our experiments that
384 produced highly dendritic olivine rims under rapid cooling (1000 °C/h). Here, however,
385 olivine rims became increasingly rounded and smooth (ripening texture) with decreasing
386 cooling rate. Notably, this change in shape seems to occur around 500 °C/h because both
387 dendritic and rounded morphologies were present in that sample. Nonetheless, it was only at
388 cooling rates of ≤50 °C/h that olivine rims began to resemble natural BO rims.
389
390 *4.1.5. Thermal conditions forming smooth olivine bars*
391 Olivine bars in natural BO chondrules are flat, sometimes segmented, and variably
392 corrugated, whereas bars obtained experimentally are always dendritic (Tsuchiyama et al.,
393 2004). Although Tsuchiyama et al. (2004) suggested that decreasing the cooling rate might
394 produce smoother bars, they considered that a reheating step was more likely to texturally
395 ripen the dendritic shape. Our results demonstrate that the cooling rate must indeed be
396 relatively slow (<10 °C/h) because experiments cooled faster (≥50 °C/h) always showed
397 dendritic crystal units, whereas those cooled at ≤10 °C/h showed more or less segmented bars
398 limited by smooth faces. Corrugation increased with decreasing cooling rate, and was
399 particularly obvious at 5 °C/h. Our reheating experiments showed that the same corrugated
400 texture can be obtained by holding the charge for several hours at 1400 °C, producing
401 segmented bars after 3 h and corrugated bars after 11–12 h. In contrast, the duration that the

charges were held at increased temperature was not long enough to produce textural ripening because pieces of dendrites were always noticeable. Therefore, our experimental results demonstrate that bars truly similar to natural BO chondrules require slow cooling (<10 °C/h) or a relatively long reheating episode (>10 h). However, reheating enriched the liquid in the olivine component, causing a second dendritic crystallisation step that is not observed within natural BO chondrules.

4.1.6. Thermal conditions forming round glass inclusions

Glass inclusions in both olivine bars and rims of natural BO chondrules are rounded or ovoid (Varela et al., 2006). In contrast, glass inclusions in olivines crystallised in rapidly cooled charges (>10 °C/h) are limited by faces that correspond to the 'negative' crystal shape that is characteristic of melt inclusions formed during rapid crystal growth (Colin et al., 2012). Tsuchiyama et al. (2004) described glass inclusions with the same shape in their rapidly cooled experiments (>500 °C/h). Therefore, our results suggest that slow cooling (< 10 °C/h) is necessary to form rounded glass inclusions. However glass inclusions obtained in reheating experiments are similarly shaped. .

4.2. Cooling conditions required to crystallise BO chondrules

Our experimental results show reproducing all the characteristics of BO chondrules (few crystals, parallel bars, rims, smooth and sometimes corrugated bars, and ovoid glass inclusions), requires slow cooling (<10 °C/h). Although reheating after fast cooling could be an alternative to slow cooling because it allows textural ripening and reproduces most of the textural characteristics of BO chondrules, reheating also results in olivine dissolution. Therefore, the chemical composition of the liquid mesostasis becomes enriched in the forsterite component, particularly MgO. The first consequence of this change in liquid

composition translates to difficulty in quenching the samples and the presence of numerous dendritic olivine crystals. The second consequence is that melt inclusion MgO contents should also increase accordingly. However, our results (Supplementary Table S2) and scarce literature data (Varela et al., 2006) show that natural BO glass inclusions always have low MgO contents (2.65 ± 1.87 wt.%). Such low-MgO glass inclusions are undersaturated in the olivine component and are compositionally very similar to glass inclusions hosted in magnesian olivines in porphyritic chondrules (Fig. 7), which are only produced through slow cooling (Faure et al., 2012; Faure, 2020). Indeed, such low MgO contents result in the equilibrium metastable crystallisation of the olivine rim around the inclusion (Faure and Tissandier, 2014). In natural BO chondrules, glassy mesostases are also olivine-undersaturated (Varela et al., 2006; Berlin, 2010), inconsistent with rapid cooling. Moreover, slow cooling can explain the lack of Fe-Mg growth zoning in bars of natural BO chondrules, in contrast to synthetic olivines crystallised under rapid cooling rates (Lofgren and Lanier, 1990; Tsuchiyama et al., 2004). Therefore, although BO chondrules might have formed during a singular cooling event or experienced an oscillatory thermal history (reheating), slow terminal cooling before quenching is necessary to obtain the true BO texture.

4.3. Implications for chondrule crystallisation

Our results on BO chondrule crystallisation have broad implications because there remains no further textural evidence for the rapid cooling of chondrules, porphyritic or not. Indeed, this result is consistent with plagioclase-bearing porphyritic chondrules that seem to require very slow cooling rates (1 °C/h) at the end of crystallisation (Wick and Jones, 2012). Moreover, the slow cooling rates obtained here for BO chondrule crystallisation are consistent with those (0.5–50 °C/h) determined for magmatic type-B Ca-Al-rich inclusions, which are considered to have experienced a similar thermal history (Jones et al., 2000). Therefore, slow

cooling rates may be common to all similar chondritic objects (Fig. 8), with important implications for the formation of the solar system.

No consensus exists on the process(es) of chondrules formation, and numerous models ranging from nebular to planetary processes have been proposed to explain why chondrules display such a wide variety of textures and chemical compositions (Desch et al., 2012; Connolly and Jones, 2016; Hewins et al., 2018). However, in all cases, it is largely accepted that chondrules resulted from the crystallisation of small beads of liquid that had already more or less crystallised within a gas. The density of chondrules in the chondrule-forming region of the gas is generally constrained based on the occurrence of compound chondrules, peculiar chondrules that resulted from chondrule-chondrule collisions while at least one of them was partially molten. Initially thought to have formed exclusively at above 1400 K (Ciesla et al., 2004), compound chondrules may have formed at lower temperatures during collisions between undercooled melt droplets (Arakawa and Nakamoto, 2016). Whatever the temperature range considered, it is generally proposed that the BO texture forms during a rapid phenomena occurring over 100–1,000 s in the gas cloud (Miura et al. 2010; Bischoff et al., 2017). However, the slow cooling rates determined herein for chondrule crystallisation suggest a longer time scale of several days, not minutes to hours, implying that the density of chondrules in the chondrule-forming region was two to four orders of magnitude lower than previously considered (Table S3). Similarly, solid:gas ratios calculated for this new time scale are larger than the canonical value (0.005), but smaller than oft-proposed values that result in too rapid a gravitational instability (Bischoff et al., 2017).

5. Conclusions

We proposed a definition of the natural BO texture that considers (i) the presence of parallel bars and rims, (ii) the fact that bars correspond to ripened dendrites, and (iii) that melt

inclusions have ovoid shapes and are olivine undersaturated. Our experimental results show that these characteristics can only be reproduced under relatively slow cooling rates (<10 °C/h); reheating scenarios cannot form true BO textures because they cause the melt to become enriched in the olivine component, producing olivine-enriched melt inclusions. Therefore, chondrule crystallisation must have occurred over days, not minutes to hours as generally suggested. These slow rates are consistent with rates determined for other chondritic objects, including plagioclase-bearing porphyritic chondrules and magmatic type-B Ca-Al-rich inclusions, suggesting that slow cooling could be common to all chondritic objects.

Acknowledgements

We thank Robert Dennen (RD Editing Services) for improving the English of the paper. We are grateful to the Muséum national d'Histoire naturelle de Paris for the Felix 1 and Sahara 00177-2 samples. This study was supported by the Programme National de Planétologie: PNP-INSU and by Région Grand Est in France through the grant provided to MA.

References

Anders, E., Grevesse, N., 1989. Abundance of the elements: Meteoritic and solar. Geochim. Cosmochim. Acta 53, 197–214.

Arakawa, S., Nakamoto, T., 2016. Compound chondrule formation via collision of supercooled droplets. Icarus 276, 102–106.

Auxerre, M., Faure, F., Lequin, D., In press. The effects of superheating and cooling rate on olivine growth in chondritic liquid. Meteorit. Planet. Sci.

Berlin, J., 2010. Mineralogy and bulk chemistry of chondrules and matrix in petrologic type 3 chondrites : implications for early solar system processes. Ph. D. Dissertation. Free University, Berlin, 233 pp.

Bischoff, A., Wurm, G., Chaussidon, M., Horstmann, M., Metzler, K., Weyrauch, M., Weinauer, J., 2017. The Allende multicompound chondrule (ACC)-Chondrule formation in a local super-dense region of the early solar system. Meteorit. Planet. Sci. 52, 906–924.

Ciesla, F. J., Lauretta, D. S., Hood, L. L., 2004. The frequency of compound chondrules and implications for chondrule formation. Meteorit. Planet. Sci. 39, 531–544.

Cohen, B. A., Hewins, R. H., Alexander, C. M. O'D., 2004. The formation of chondrules by open-system melting of nebular condensates. Geochim. Cosmochim. Acta 68, 1661–1675.

Colin, A., Faure, F., Burnard, P., 2012. Timescales of convection in magma chambers below the Mid-Atlantic ridge from melt inclusions investigation. Contrib. Mineral. Petrol.

164, 677–691.

Connolly, H. C. Jr., Desch, S. J., 2004. On the origin of the "kleine Kügelchen" called chondrules. Chem. Erde 64, 95–125.

Connolly, H. C. Jr., Hewins, R. H., 1991. The influence of bulk composition and dynamic melting conditions on olivine chondrule textures. Geochim. Cosmochim. Acta 55, 2943–2950.

Connolly, H. C. Jr., Hewins, R. H., 1995. Chondrules as products of dust collisions with totally molten droplets within a dust-rich nebular environment: An experimental investigation. Geochim. Cosmochim. Acta 59, 3231–3246.

Connolly, H. C. Jr., Jones, B. D., Hewins, R. H., 1998. The flash melting of chondrules: An experimental investigation into the melting history and physical nature of chondrule precursors. Geochim. Cosmochim. Acta 62, 2725–2735.

Connolly, H. C. Jr., Jones, R. H., 2016. Chondrules: The canonical and noncanonical views. J. Geophys. Res. Planets 121, 1885–1899.

DeHart, J. M., Lofgren, G. E., 1996. Experimental studies of group A1 chondrules. Geochim. Cosmochim. Acta 60, 2233–2242.

Desch, S. J., Morris, M. A., Connolly, Jr., H. C., Boss, A. P., 2012. The importance of experiments: Constraints on chondrule formation models. Meteorit. Planet. Sci. 47, 1139–1156.

Donaldson, C. H., 1976. An experimental investigation of olivine morphology. Contrib. Mineral. Petrol. 57, 187–213.

Faure, F., 2020. Early silica crust formation in planetesimals by metastable silica-rich liquid immiscibility or cristobalite crystallisation: the possible origin of silica-rich chondrules. Scientific Reports 10, 4765. doi.org/10.1038/s41598-020-61806-5

Faure, F., Arndt, N., Libourel, G., 2006. Formation of spinifex texture in Komatiites: an

552 experimental study. J. Petrol. 47, 1591–1610.
553 Faure, F., Tissandier, L., 2014. Contrasted liquid lines of descent revealed by olivine-hosted
554 melt inclusions and the external magma. J. Petrol. 35, 1779–1798.
555 Faure, F., Tissandier, L., Libourel, G., Mathieu, R., Welsch, B., 2012. Origin of glass
556 inclusions hosted in magnesian porphyritic olivines chondrules: Deciphering
557 planetesimal compositions. Earth Planet. Sci. Lett. 319–320, 1–8.
558 Faure, F., Trolliard, G., Nicollet, C., Montel, J.M., 2003a. A developmental model of olivine
559 morphology as a function of the cooling rate and the degree of undercooling. Contrib.
560 Mineral. Petrol. 145, 251–263.
561 Faure, F., Trolliard, G., Soulestin, B., 2003b. TEM investigation of forsterite dendrites. Am.
562 Miner. 88,1241–1250.
563 First, E. C., Leonhardi T. C., Hammer, J. E., 2020. Effects of superheating magnitude on
564 olivine growth. Contrib. Mineral. Petrol. 175, 13.
565 Gooding, J. L., Keil, K., 1981. Relative abundances of chondrule primary textural types in
566 ordinary chondrites and their bearing on conditions of chondrule formation.
567 Meteoritics 16, 17–42.
568 Hewins, R.H., Klein, L.C.,Fasano, B.V., 1981. Conditions of formation of pyroxene
569 excentroradial chondrules. Proc. Lunar Planet. Sci. 12, 1123-1133.
570 Hewins, R. H., Radomsky, P. M., 1990. Temperature conditions for chondrule formation.
571 Meteoritics 25, 309–318.
572 Hewins, R.H., Condie, C., Morris, M., Richardson, M.L.A., Ouellette, N., Metcalf, M., 2018.
573 Thermal history of CB_b chondrules and cooling rate distributions of ejecta plumes.
574 Astrophys. J. 855:L17, 1-7.
575 Jambon, A., Lussiez, P., Clocchiatti, R., 1992. Olivine growth rates in a tholeiitic basalt: An
576 experimental study of melt inclusions in plagioclase. Chem. Geol. 96, 277–287.

577 Jones, R. H., Lee, T., Connolly, H. C. Jr., Love, S. G., Shang, H., 2000. Formation of
578 chondrules and CAIs: Theory vs. observation, in: Mannings, V., Boss, A. P., Russell,
579 S. S. (Eds.), Protostars and Planets IV. Univ. of Arizona Press, Tucson, pp. 927–962.
580 Jones, R. H., Villeneuve, J., Libourel, G., 2018. Thermal histories of chondrules: Petrologic
581 observations and experimental constraints, in: Russell, S. S., Connolly, H. C. Jr., Krot,
582 A. N. (Eds.) Chondrules: Records of protoplanetary disk processes. Cambridge
583 University Press, Cambridge, pp. 57–90.
584 Kennedy, A. K., Lofgren, G. E., Wasserburg, G. J., 1993. An experimental study of trace
585 element partitioning between olivine, orthopyroxene and melt in chondrules:
586 equilibrium values and kinetic effects. Earth Planet. Sci. Lett. 115, 177–195.
587 Kirkpatrick, J. R., 1983 Theory of nucleation in silicate melts. Am. Miner. 68, 66–77.
588 Libourel, G., Portail, M., 2018. Chondrules as direct thermochemical sensors of solar
589 protoplanetary disk gas. Sci. Adv. 4, eaar3321.
590 Lofgren, G., 1989. Dynamic crystallization of chondrule melts of porphyric olivine
591 composition: Textures experimental and natural. Geochim. Cosmochim. Acta 53, 461–
592 470.
593 Lofgren, G., Lanier, A. B., 1990. Dynamic crystallization of barred olivine chondrules.
594 Geochim. Cosmochim. Acta 54, 3537–3551.
595 Lofgren, G., Russell, W. J., 1986. Dynamic crystallization of chondrule melts of porphyritic
596 and radial pyroxene composition. Geochim. Cosmochim. Acta 50, 1715–1726.
597 Miura, H., Tanaka, K.K., Yamamoto, T., Nakamoto, T., Yamada, J., Tsukamoto, K., Nozawa,
598 J., 2010. Formation of cosmic crystals in highly supersaturated silicate vapor produced
599 by planetesimal bow shocks. Astrophys. J. 719, 642-654.
600 Miura, H., Yokoyama, E., Nagashima, K., Tsukamoto, K., Srivastava, A., 2011. A new
601 constraint for chondrule formation: condition for the rim formation of barred-olivine

602 textures. Earth Planets Space 63, 1087-1096.
603 Nagahara, H., 1996. Evaporation induced isothermal crystallization of silicate melt. Lunar
604 Planet. Sci. 27, 927–928.
605 Noguchi, T., 2002. Estimation of three-dimensional internal structures of some barred olivine
606 chondrules in Allende (CV3) chondrite. Antatct. Meteorite Res. 15**,** 59–77.
607 Radomsky, P. M., Hewins, R. H., 1990. Formation conditions of pyroxene-olivine and
608 magnesian olivine chondrules. Geochim. Cosmochim. Acta 54, 3475–3490.
609 Rubin, A. E., 2000. Petrologic, geochemical and experimental constraints on models of
610 chondrule formation. Earth Sci. Rev. 50, 3–27.
611 Tsuchiyama, A., Kawabata, T., Kondo, M., Uesugi, K., Nakano, T., Suzuki, Y., Yagi, N.,
612 Umetani, K., Shirono, S., 2000. Spinning chondrules deduced from their three-
613 dimensional structures by X-ray CT method. Lunar Planet. Sci. 31, 1566.
614 Tsuchiyama, A., Nagahara, H., Kushiro, I., 1980. Experimental reproduction of textures of
615 chondrules. Earth Planet. Sci. Lett. 48, 155–165.
616 Tsuchiyama, A., Osada, Y., Nakano, T., Uesugi, K., 2004. Experimental reproduction of
617 classic barred olivine chondrules: Open-system behavior of chondrule formation.
618 Geochim. Cosmochim. Acta 68, 653–672.
619 Tsukamoto, K., Kobatake, H. Nagashima, K. Satoh, H., Yurimoto, H., 2001. Crystallization
620 of Cosmic Materials in Microgravity. Lunar Planet. Sci. 32, 1846–1847.
621 Varela, M. E., Kurat, G., Zinner, E., 2006. The primary liquid condensation model and the
622 origin of barred olivine chondrules. Icarus 184, 344–364.
623 Weisberg, M. K., 1987. Barred olivine chondrules in ordinary chondrules: petrologic
624 constraints and implications. J. Geophys. Res. 92, 663–678.
625 Wick, M., Jones, R. H., 2012. Formation conditions of plagioclase-bearing type I chondrules
626 in CO chondrites: A study of natural samples and experimental analogs. Geochim.

Cosmochim. Acta 98, 140–159.

Author contributions

F.F. and V.C. designed the study and experiments. F.F. and M.A. conducted the analytical work. All authors participated in the interpretation of the data. F.F. wrote the manuscript with input from M.A. and V.C.

Competing interests

The authors declare no competing interests.

Figure captions

Fig. 1. A classic BO chondrule from the Felix (CO3) carbonaceous chondrite. (a) Optical image under transmitted light, displaying that the BO chondrule is rimmed by a shell of olivine and contains parallel bars of olivine set in glass. (b) Enlarged view of the square in (a), highlighting ovoid glass inclusions (Gi) in olivine (ol).

Fig. 2. Backscattered electron (BSE) images of dynamic crystallisation experiments cooled to (a–e) 1200 °C or (f) 1210 °C at decreasing cooling rates (Table 1). (a) Experiment 23-N258; (b) experiment 24-N259; (c) experiment 29-N262; (d) experiment 31-N261; (e) experiment 34-N270; (f) experiment 35-N272.

652 **Fig. 3.** BSE images of experimental charges showing that the dendritic shapes of rods
653 decrease with decreasing cooling rate. (a) Dove-shaped units ('wings' indicated by arrows)
654 constituting dendritic rods are obviously visible in rapidly cooled charges (here, experiment
655 30-N299). (b) Only pieces of the 'wings' of dove units are observable in charges cooled more
656 slowly (experiment 31-N261).
657
658 **Fig. 4.** BSE images of olivine rims as a function of cooling rate. (a) Experiment 26-N268; (b)
659 experiment 29-N262; (c) experiment 31-N261 (d) experiment 34-N270; (e) enlarged view of
660 the square in (d) showing ovoid glass inclusions (Gi) hosted in the olivine rim. (f) Experiment
661 35-N272; in addition to olivine crystals, this charge contained euhedral spinel crystals.
662
663 **Fig. 5.** BSE images of experimental charges showing minimal textural ripening during
664 periods of isothermal heating during dynamic crystallisation experiments. (a) Experiment 27-
665 N260 was held isothermally at 1200 °C for 2 h after rapid cooling. (b) Enlarged view of the
666 rectangle in (a), showing that rods are always dendritic. (c) After rapid cooling at 500 °C/h,
667 experiment 28-N263 was held isothermally at 1200 °C for 4 h before a second rapid constant
668 cooling step (300 °C/h) down to 900 °C, at which temperature the charge was held
669 isothermally for 62 h. This long duration at low temperature can explain the spherulitic
670 texture in the mesostasis. (d) Enlarged view of the rectangle in (c), showing that glass
671 inclusions (Gi) hosted in olivine bars have 'negative' skeletal crystal shapes.
672
673 **Fig. 6.** BSE images of experimental charges showing textural ripening due to reheating to
674 1400 °C after rapid cooling by (a–f) 500 °C/h or (g–h) 50 °C/h. (a) Experiment 36-N264 was
675 reheated to 1400 °C and immediately quenched. (b) Enlarged view of the rectangle in (a),
676 showing that bars are still dendritic and quench dendrites developed on the rim. (c)

Experiment 37-N265 was reheated to 1400 °C and held for 3 h; this charge displays the true BO texture with flat olivine bars. (d) Enlarged view of the rectangle in (c), showing that quench dendritic rods developed between the smooth surfaces of the well-developed rods. (e) Experiment 38-N266 was reheated to 1400 °C and held for 12.5 h. (f) Enlarged view of the rectangle in (e), showing dendritic overgrowths developed on segmented rods. (g) Experiment 39-N271 was cooled at 50 °C/h then reheated to 1400 °C for 11 h. (h) Enlarged view of the rectangle in (g), showing that, even with a slower initial cooling rate, quench overgrowths are always present in reheating experiments.

Fig. 7. Normative compositions of olivine-hosted glass inclusions in BO chondrules projected onto the forsterite-anorthite-silica plane. Analysed glass inclusions in natural BO chondrules (open red squares, this study; filled red circles, Varela et al., 2006) show the same compositional variability as olivine-hosted glass inclusions in porphyritic chondrules (Al-rich, Al-poor, Na-rich, and Si-rich glass inclusions, represented by their respective coloured fields). Regardless of chondrule texture, the compositions of glass inclusions plot outside the stability field of their host forsterite.

Fig. 8. Cooling rates used to experimentally reproduce chondrule textures. Various chondrule textures (BO, barred olivine; PO, porphyritic olivine and porphyritic olivine-pyroxene; RP, radial pyroxene) can be reproduced over large ranges of cooling rates, except BO chondrules, which are traditionally interpreted to result from rapid cooling (red rectangle; data compilation after Desch et al., 2012; Jones et al., 2018). However, those experiments never reproduced the true BO texture, which our slow cooling results (red circles) reproduce well, thus challenging the traditional assumption that chondrules crystallised under rapid cooling. Consequently, all chondrule textures can be explained by slow cooling rates (<10 °C/h),

consistent with those envisioned for magmatic type-B Ca-Al-rich inclusions (Jones et al., 2000).

Table 1. Summary of run conditions and products in isothermal and dynamic crystallisation experiments.

Table 2. Summary of run conditions and products in reheating experiments.

Supplementary Material

Fig. S1. BSE images of isothermal experimental charges showing dendritic crystal textures produced during air quenching. (a) Experiment 8-N180 was held isothermally at 1450 °C for 16 h before quenching in air and shows both dendritic rods and polyhedral-skeletal olivine crystals. (b) Experiment 7-N173 was held isothermally at 1450 °C for 7 h before quenching in air and shows dendritic parallel rods of olivine.

Fig. S2. BSE images of experimental charges showing dendritic crystal textures produced during air quenching. (a) Dynamic crystallisation experiment 40-N269 was cooled to 1200 °C and reheated to 1500 °C; it displays numerous thin dendrites of olivine in the glass mesostasis. (b) Isothermal experiment 12-N194 was held at 1500 °C for 2 h before air

quenching and shows a dendritic texture similar to that in (a). (c) Isothermal experiment 16-N234 was held at 1600 °C for 5 minutes before air quenching, and shows a dendritic texture similar to those in (a) and (b).

Table S1. Chemical compositions (EDS analyses, in wt.%) of olivines crystallized during dynamic crystallization experiments.

Table S2. Chemical compositions (EDS analyses, in wt.%) and normative mineralogy of glass inclusions in barred olivine chondrules.

Table S3. Chondrule number density and solid:gas ratio as a function of cooling time scale. T_{in}, initial chondrule temperature; T_{end}, the lowest temperature at which melt could have been present in the chondrule.

n: the local number density of chondrules can be estimated by $n = \frac{0.8}{t_{cool}\, r_p^2\, v}$, where r_p = 0.5 mm is the chondrule radius; v is the collision velocity, which typically varies between 0.5 and 5 m/s; and t_{cool} is the cooling time, which corresponds to the time elapsed before chondrules were too cold to stick together (Bischoff et al., 2017).

ρ_s: the initial local mass density of all chondrule precursor materials can be calculated as $\rho_s = 3.3\, \rho_p\, \frac{r_p}{t_{cool} v}$, where the individual chondrule mass density ρ_s = 3,500 kg/m^3 (Bischoff et al., 2017). The ratio between precursor density and gas density is calculated assuming a mass density of 1.4×10^{-6} kg/m^3 at 1 AU in a minimum-mass solar nebula (Hayashi et al., 1985).

Supplemental reference list

751 Hayashi, C., Nakazawa, K., Nakagawa, Y., 1985. The formation of the solar system, in: Black,
752 D. C., Mathews, M. (Eds.) Protostars and planets II. Univ. of Arizona Press, Tucson,
753 pp. 1100–1153.
754

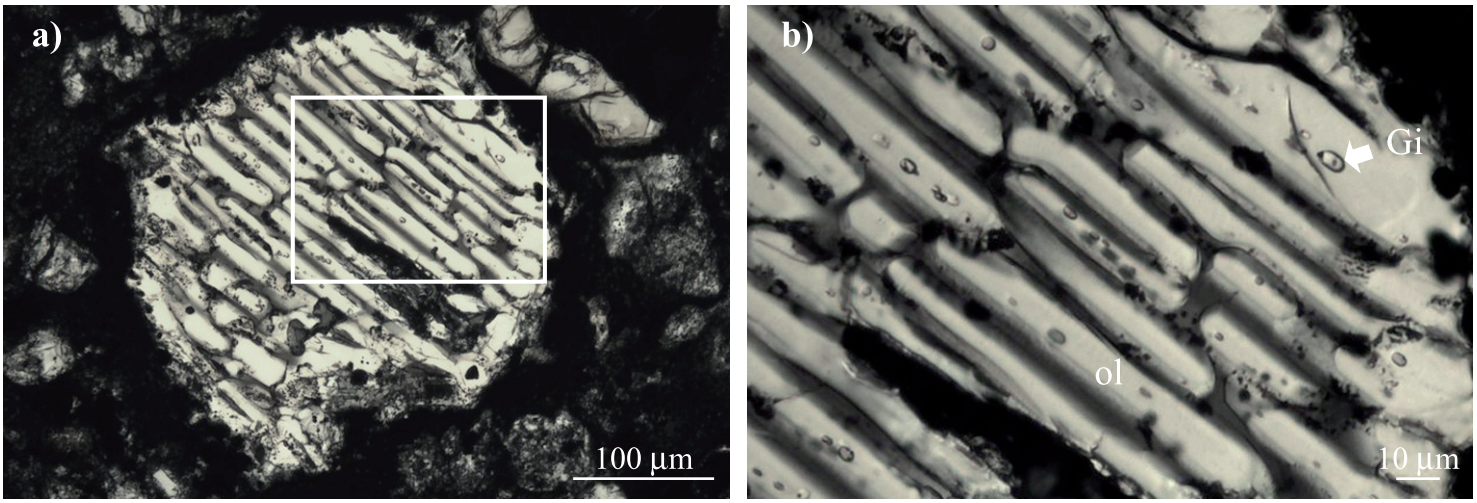

Fig. 1. A classic BO chondrule from the Felix (CO3) carbonaceous chondrite. (a) Optical image under transmitted light, displaying that the BO chondrule is rimmed by a shell of olivine and contains parallel bars of olivine set in glass. (b) Enlarged view of the square in (a), highlighting ovoid glass inclusions (Gi) in olivine (ol).

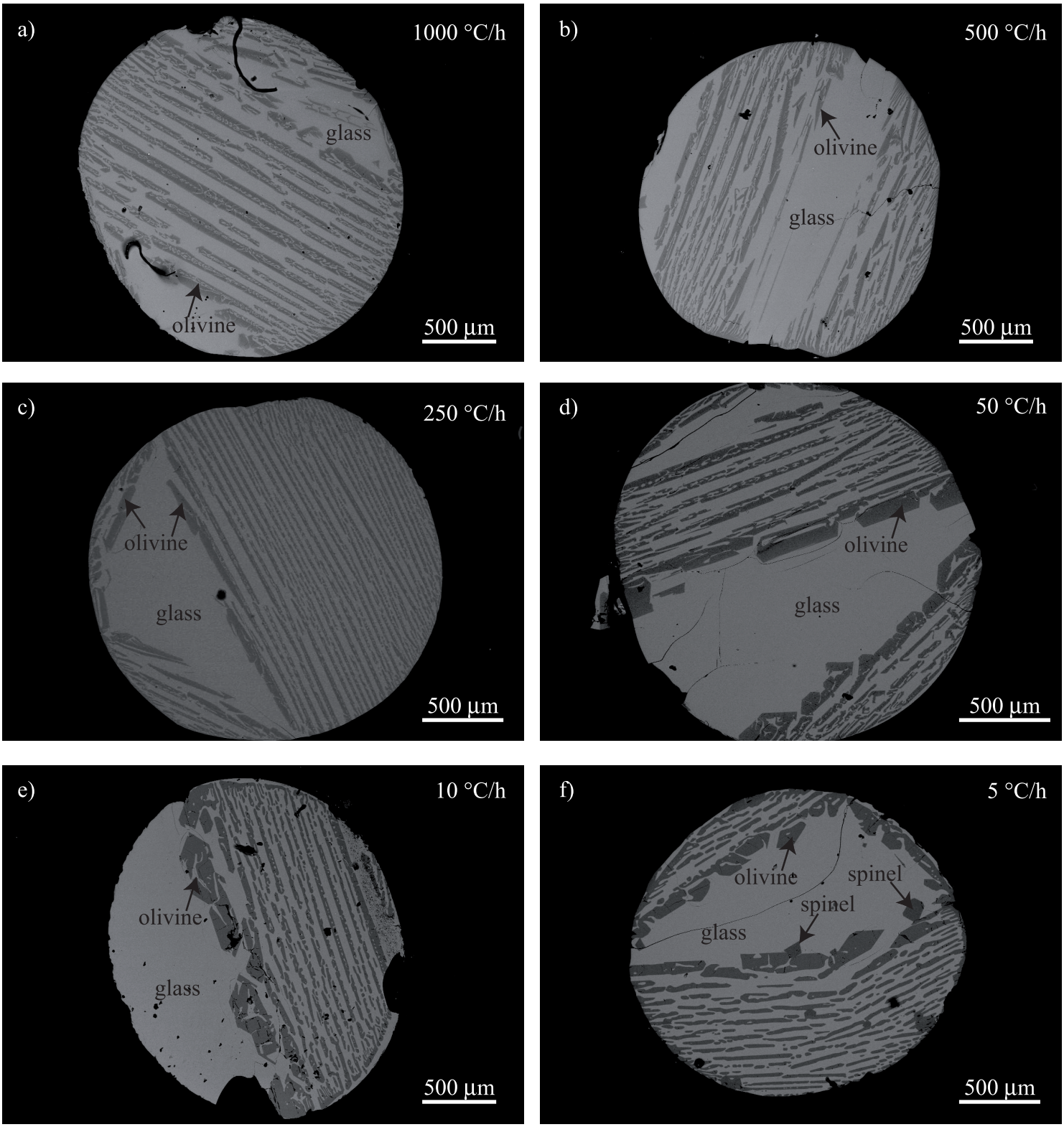

Fig. 2. Backscattered electron (BSE) images of dynamic crystallisation experiments cooled to (a–e) 1200 °C or (f) 1210 °C at decreasing cooling rates (Table 1). (a) Experiment 23-N258; (b) experiment 24-N259; (c) experiment 29-N262; (d) experiment 31-N261; (e) experiment 34-N270; (f) experiment 35-N272.

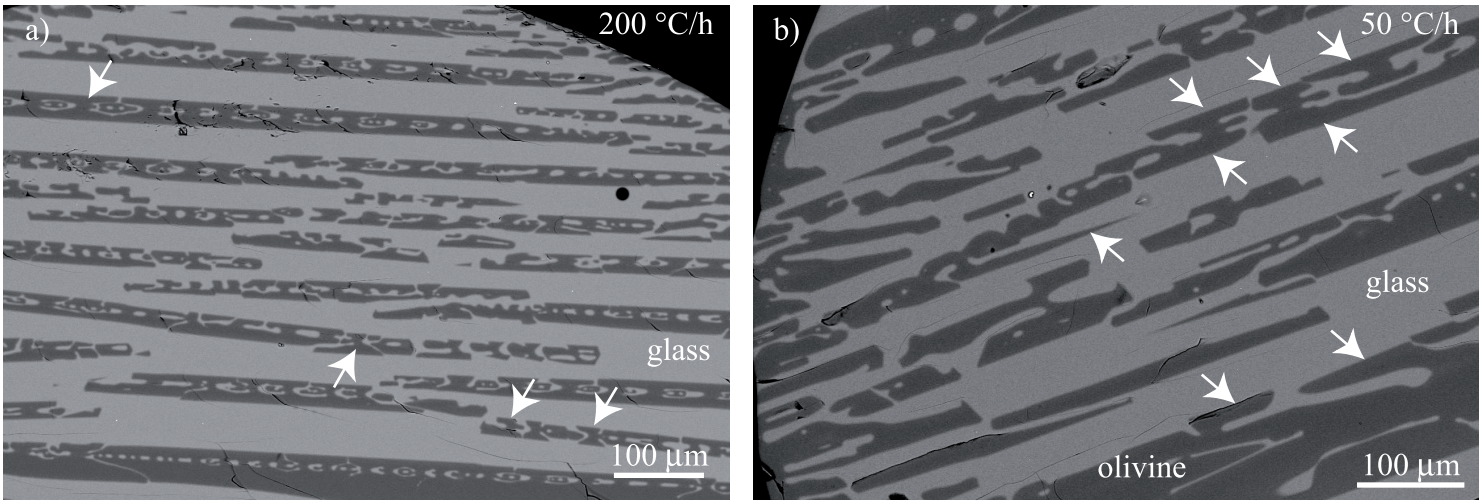

Fig. 3. BSE images of experimental charges showing that the dendritic shapes of rods decrease with decreasing cooling rate. (a) Dove-shaped units (‘wings’ indicated by arrows) constituting dendritic rods are obviously visible in rapidly cooled charges (here, experiment 30-N299). (b) Only pieces of the ‘wings’ of dove units are observable in charges cooled more slowly (experiment 31-N261).

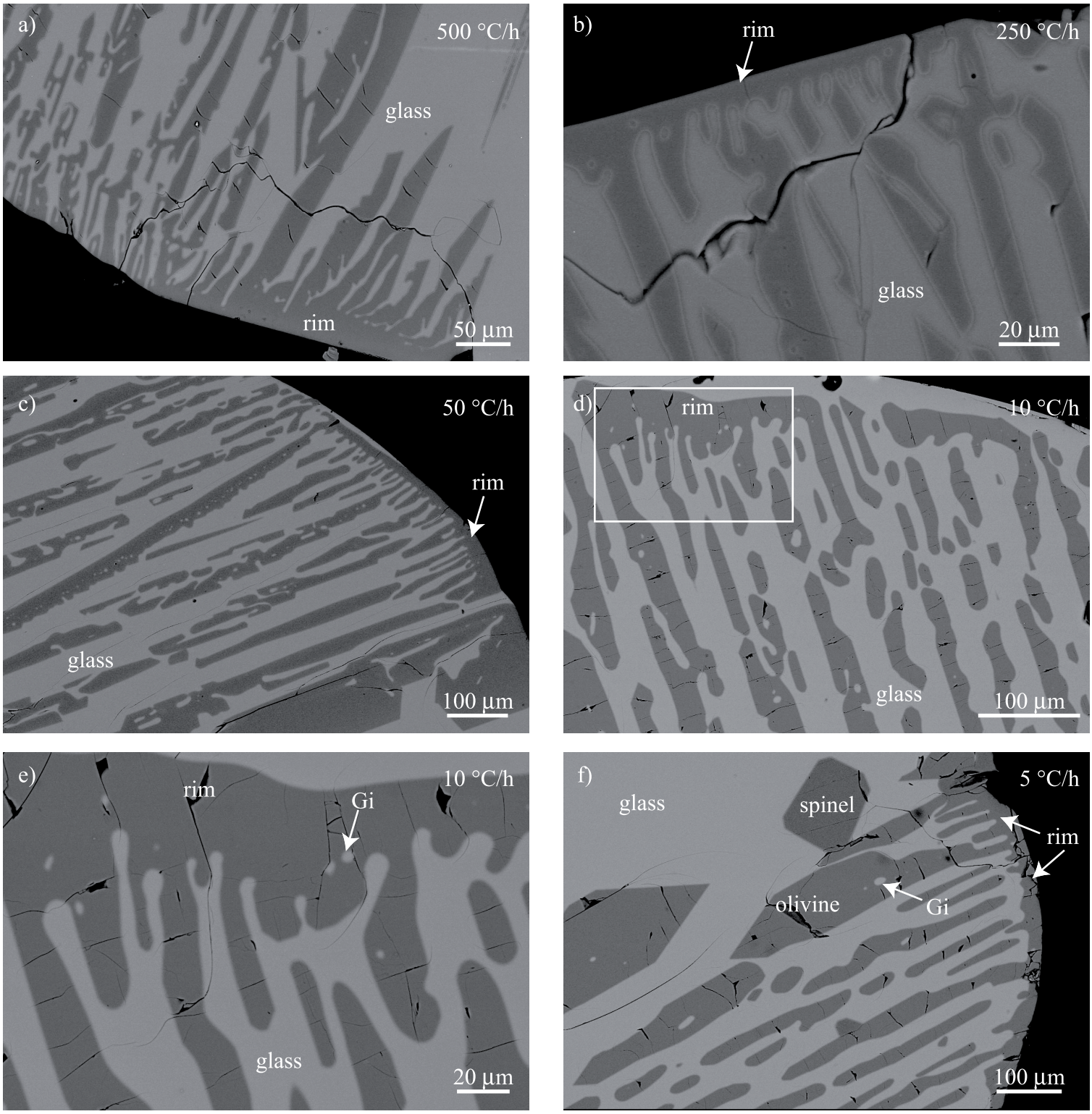

Fig. 4. BSE images of olivine rims as a function of cooling rate. (a) Experiment 26-N268; (b) experiment 29-N262; (c) experiment 31-N261 (d) experiment 34-N270; (e) enlarged view of the square in (d) showing ovoid glass inclusions (Gi) hosted in the olivine rim. (f) Experiment 35-N272; in addition to olivine crystals, this charge contained euhedral spinel crystals.

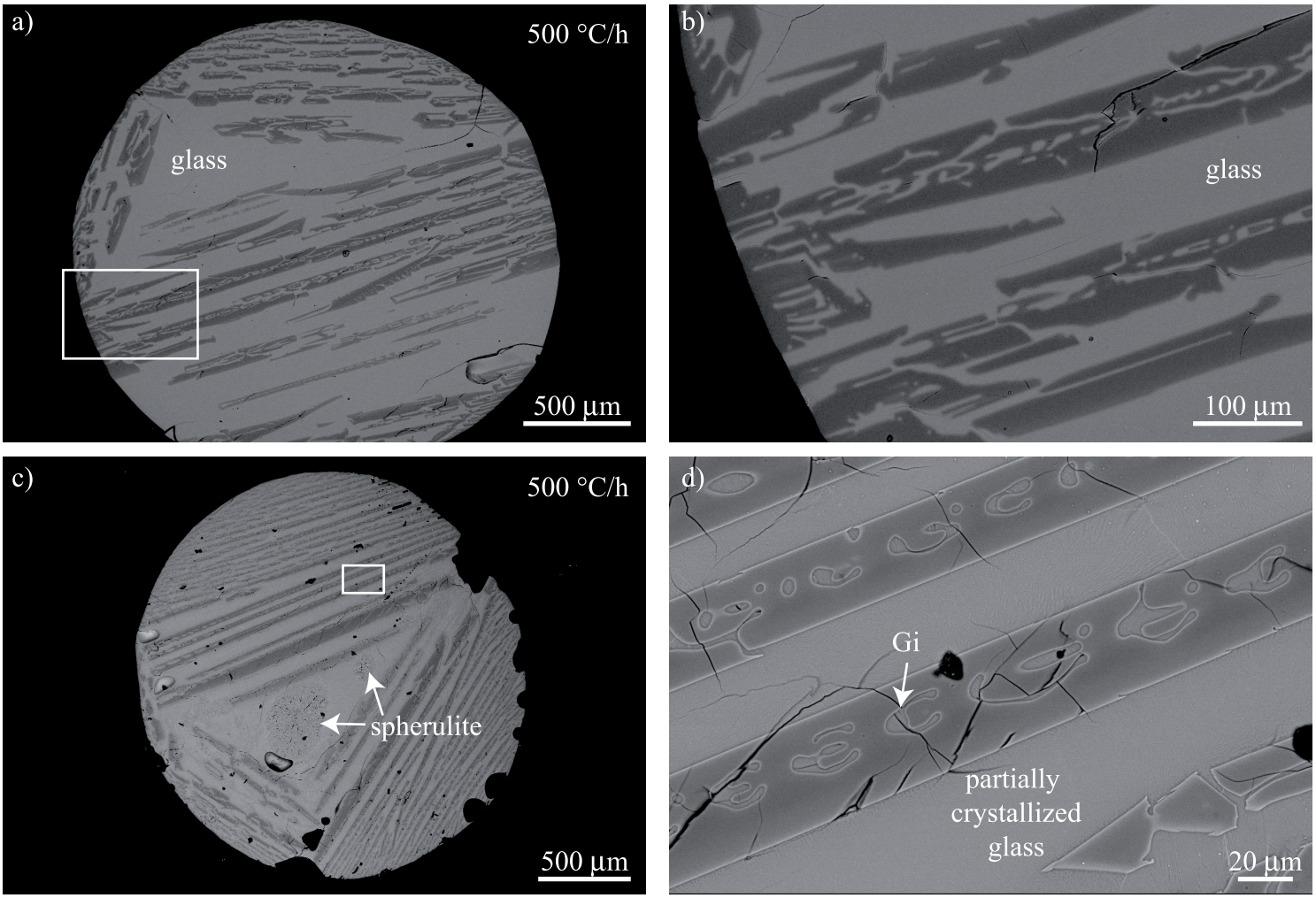

Fig. 5. BSE images of experimental charges showing minimal textural ripening during periods of isothermal heating during dynamic crystallisation experiments. (a) Experiment 27-N260 was held isothermally at 1200 °C for 2 h after rapid cooling. (b) Enlarged view of the rectangle in (a), showing that rods are always dendritic. (c) After rapid cooling at 500 °C/h, experiment 28-N263 was held isothermally at 1200 °C for 4 h before a second rapid constant cooling step (300 °C/h) down to 900 °C, at which temperature the charge was held isothermally for 62 h. This long duration at low temperature can explain the spherulitic texture in the mesostasis. (d) Enlarged view of the rectangle in (c), showing that glass inclusions (Gi) hosted in olivine bars have 'negative' skeletal crystal shapes.

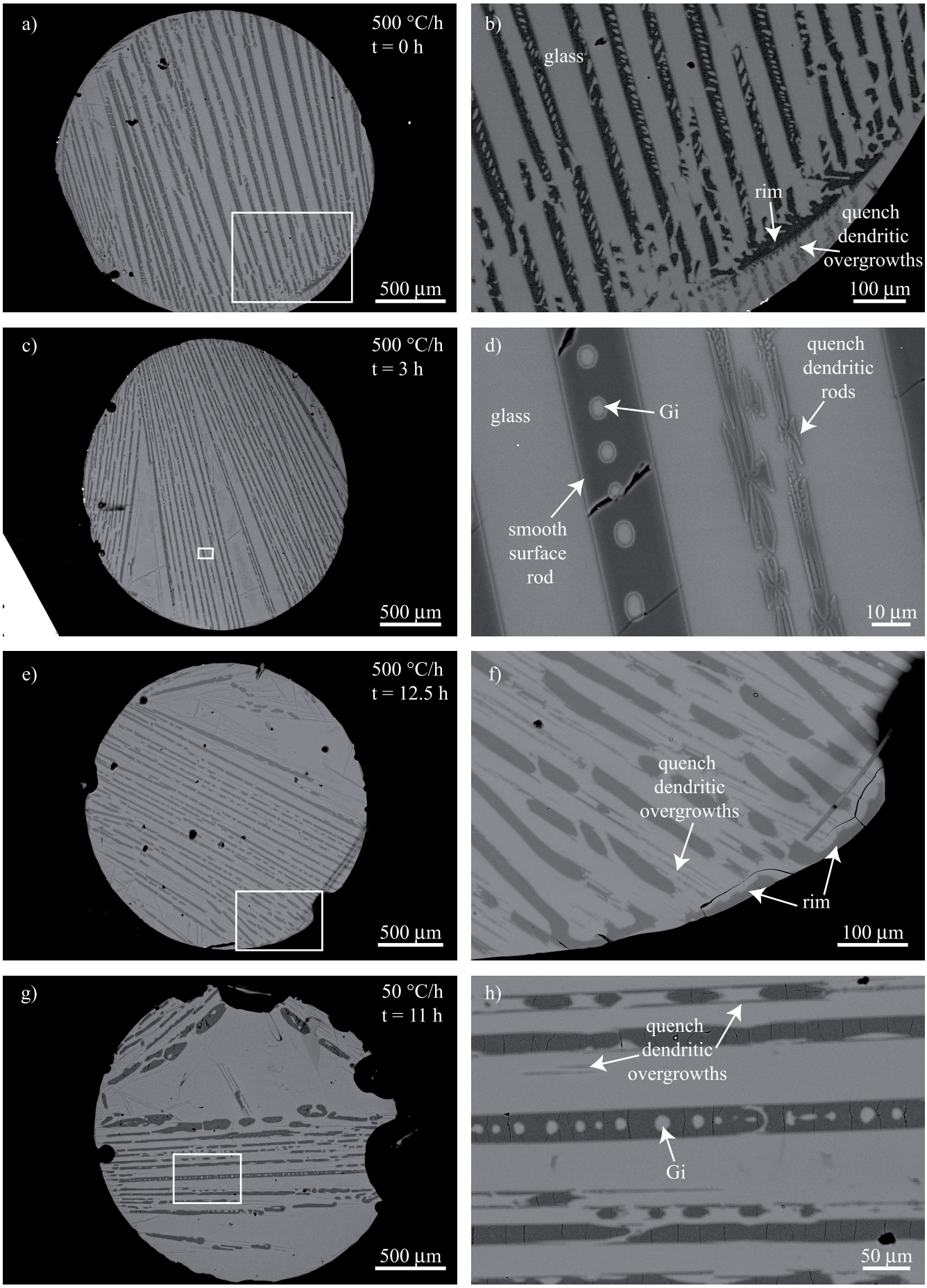

Fig. 6. BSE images of experimental charges showing textural ripening due to reheating to 1400 °C after rapid cooling by (a–f) 500 °C/h or (g–h) 50 °C/h. (a) Experiment 36-N264 was reheated to 1400 °C and immediately quenched. (b) Enlarged view of the rectangle in (a), showing that bars are still dendritic and quench dendrites developed on the rim. (c) Experiment 37-N265 was reheated to 1400 °C and held for 3 h; this charge displays the true BO texture with flat olivine bars. (d) Enlarged view of the rectangle in (c), showing that quench dendritic rods developed between the smooth surfaces of the well-developed rods. (e) Experiment 38-N266 was reheated to 1400 °C and held for 12.5 h. (f) Enlarged view of the rectangle in (e), showing dendritic overgrowths developed on segmented rods. (g) Experiment 39-N271 was cooled at 50 °C/h then reheated to 1400 °C for 11 h. (h) Enlarged view of the rectangle in (g), showing that, even with a slower initial cooling rate, quench overgrowths are always present in reheating experiments.

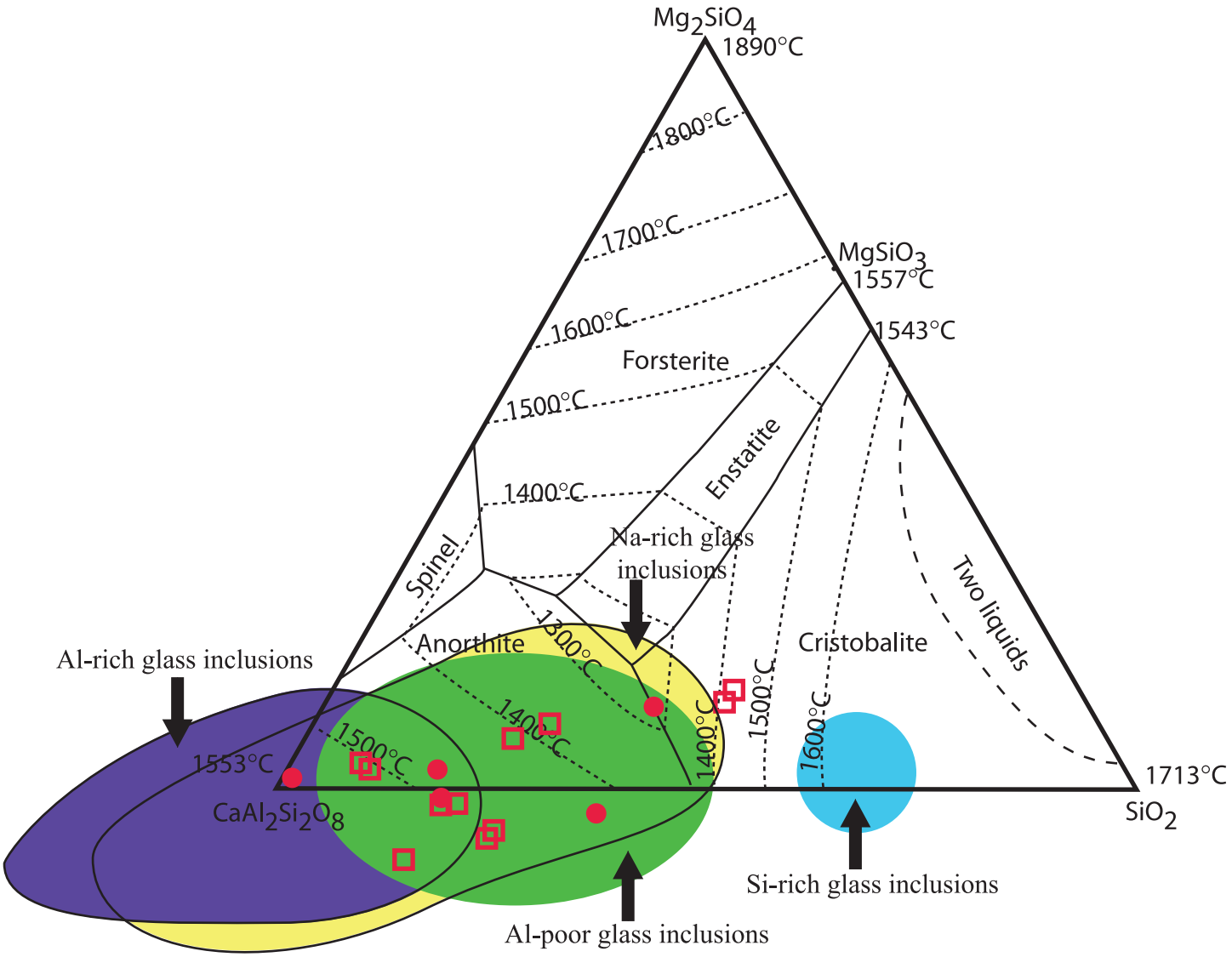

Fig. 7. Normative compositions of olivine-hosted glass inclusions in BO chondrules projected onto the forsterite-anorthite-silica plane. Analysed glass inclusions in natural BO chondrules (open red squares, this study; filled red circles, Varela et al., 2006) show the same compositional variability as olivine-hosted glass inclusions in porphyritic chondrules (Al-rich, Al-poor, Na-rich, and Si-rich glass inclusions, represented by their respective coloured fields). Regardless of chondrule texture, the compositions of glass inclusions plot outside the stability field of their host forsterite.

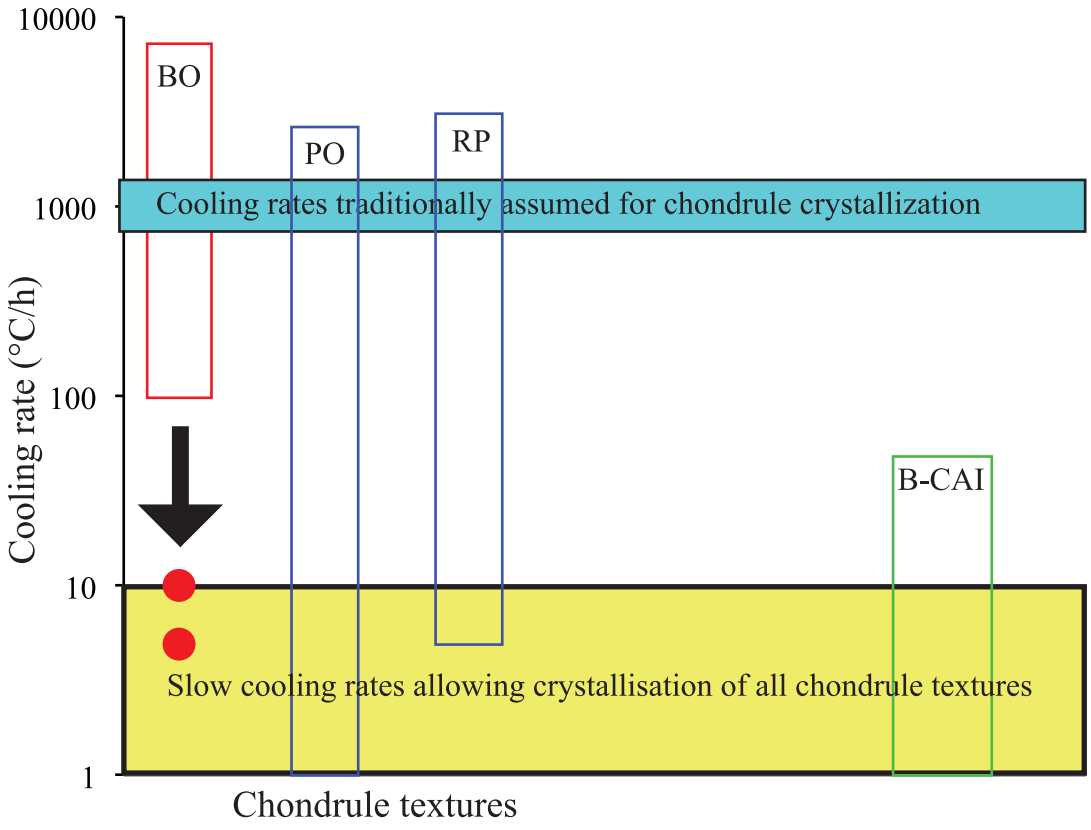

Fig. 8. Cooling rates used to experimentally reproduce chondrule textures. Various chondrule textures (BO, barred olivine; PO, porphyritic olivine and porphyritic olivine- pyroxene; RP, radial pyroxene) can be reproduced over large ranges of cooling rates, except BO chondrules, which are traditionally interpreted to result from rapid cooling (red rectangle; data compilation after Desch et al., 2012; Jones et al., 2018). However, those experiments never reproduced the true BO texture, which our slow cooling results (red circles) reproduce well, thus challenging the traditional assumption that chondrules crystallised under rapid cooling. Consequently, all chondrule textures can be explained by slow cooling rates (<10 °C/h), consistent with those envisioned for magmatic type-B Ca-Al-rich inclusions (Jones et al., 2000).

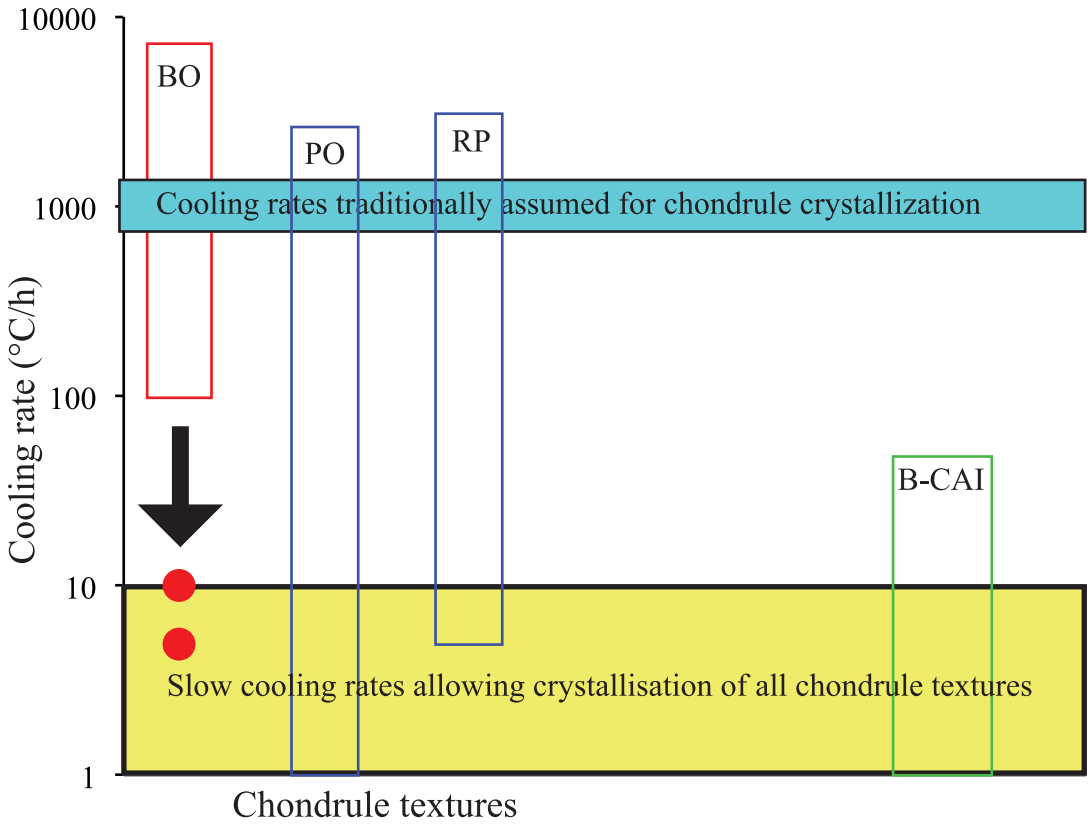

Fig. 8. Cooling rates used to experimentally reproduce chondrule textures. Various chondrule textures (BO, barred olivine; PO, porphyritic olivine and porphyritic olivine- pyroxene; RP, radial pyroxene) can be reproduced over large ranges of cooling rates, except BO chondrules, which are traditionally interpreted to result from rapid cooling (red rectangle; data compilation after Desch et al., 2012; Jones et al., 2018). However, those experiments never reproduced the true BO texture, which our slow cooling results (red circles) reproduce well, thus challenging the traditional assumption that chondrules crystallised under rapid cooling. Consequently, all chondrule textures can be explained by slow cooling rates (<10 °C/h), consistent with those envisioned for magmatic type-B Ca-Al-rich inclusions (Jones et al., 2000).

Table 1. Summary of run conditions and products in isothermal and dynamic crystallisation experiments.

Run n°	$T_{starting}$ (°C)	dT/dt (°C/h)	Dwell time before quench (min)	T_{quench} (°C)	Nb cx	Run products (textures)
Isothermal crystallisation experiments						
1-N171	1450	0	5	1450	nd	gl, Fe-cx, fo (p, s)
2-N170	1450	0	15	1450	nd	gl, Fe-cx, fo (p, s, d)
3-N165	1450	0	30	1450	nd	gl, fo (p, s)
4-N168	1450	0	60	1450	nd	gl, fo (p, s, d)
5-N169	1450	0	120	1450	nd	gl, fo (p, s, d)
6-N174	1450	0	300	1450	nd	gl, fo (p, s, d)
7-N173	1450	0	420	1450	nd	gl, fo (p, s, d)
8-N180	1450	0	960	1450	nd	gl, fo (p, s, d)
9-N193	1500	0	5	1500	nd	gl, Fe-cx, fo (p, s, d)
10-N191	1500	0	15	1500	nd	gl, fo (d)
11-N192	1500	0	30	1500	nd	gl, fo (d)
12-N194	1500	0	120	1500	nd	gl, fo (d)
13-N221	1500	0	180	1500	nd	gl, fo (d)
14-N195	1500	0	300	1500	nd	Ca-Al cx
15-N196	1500	0	420	1500	nd	Ca-Al cx
16-N234	1600	0	5	1600	nd	gl, fo (d)
17-N235	1600	0	15	1600	nd	gl, fo (d)
18-N236	1600	0	30	1600	nd	gl, fo (d)
19-N237	1600	0	60	1600	nd	gl, fo (d)
20-N238	1600	0	120	1600	82	gl, fo (d)
21-N241	1600	0	180	1600	nd	gl, fo (d)
22-N239	1600	0	300	1600	nd	gl, fo (d)
Dynamic crystallisation experiments						
23-N258	1600	1000	0	1200	4	gl, fo (FBO)
24-N259	1600	500	0	1200	1	gl, fo (FBO)
25-N267	1600	500	0	1400	62	gl, fo (d)
26-N268	1600	500	0	1300	5	gl, fo (FBO)
27-N260	1600	500	120	1200	3	gl, fo (FBO)
28-N263*	(i) 1600 (ii) 1200	500 300	240 3720	1200 900	3	gl, fo (FBO)
29-N262	1600	250	0	1200	4	gl, fo (FBO)
30-N299	1600	200	0	1200	4	gl, fo (FBO)
31-N261	1600	50	0	1200	3	gl, fo (FBO)
32-N274	1600	50	0	1400	48	gl, fo (d)
33-N273	1600	50	0	1300	3	gl, fo (FBO)
34-N270	1600	10	0	1200	1	gl, fo (TBO)
35-N272	1600	5	0	1210	3	gl, sp, fo (TBO)

Nb cx, number of crystals; nd, not determined.

Phase abbreviations: gl, glass; sp, spinel; fo, forsterite; Fe-cx, iron-rich oxide crystal; Ca-Al cx, Ca-Al-rich crystal.

Textural abbreviations: p, polyhedral crystal; s, skeletal crystal; d, dendritic crystal; FBO, false barred olivine (dendritic olivine bars, olivine rim, non-ovoid glass inclusions); TBO, true barred olivine (flat olivine bars, olivine rim, ovoid glass inclusions).

*Experiment 28-N263 was (i) rapidly cooled to 1200 °C at 500 °C/h and held for 4 h, then (ii) rapidly cooled to 900 °C at 300 °C/h and held for 62 h before the air quench.

Table 2. Summary of run conditions and products in reheating experiments.

Run n°	$T_{starting}$ (°C)	dT/dt (°C/h)	Dwell temperature (°C)	Reheating temperature (°C)	Dwell time before quench (h)	Number of crystals	Run products (textures)
36-N264	1600	500	1200	1400	0	1	gl, fo (FBO)
37-N265	1600	500	1200	1400	3	4	gl, fo (TBO)
38-N266	1600	500	1200	1400	12.5	3	gl, fo (TBO)
39-N271	1600	50	1200	1400	11	4	gl, fo (TBO)
40-N269	1600	500	1200	1500	0	46	gl, fo (d)

Phase abbreviations: gl, glass; fo, forsterite.
Textural abbreviations: d, dendritic crystal; FBO, false barred olivine (dendritic olivine bars, olivine rim, non-ovoid glass inclusions); TBO, true barred olivine (flat olivine bars, olivine rim, ovoid glass inclusions).

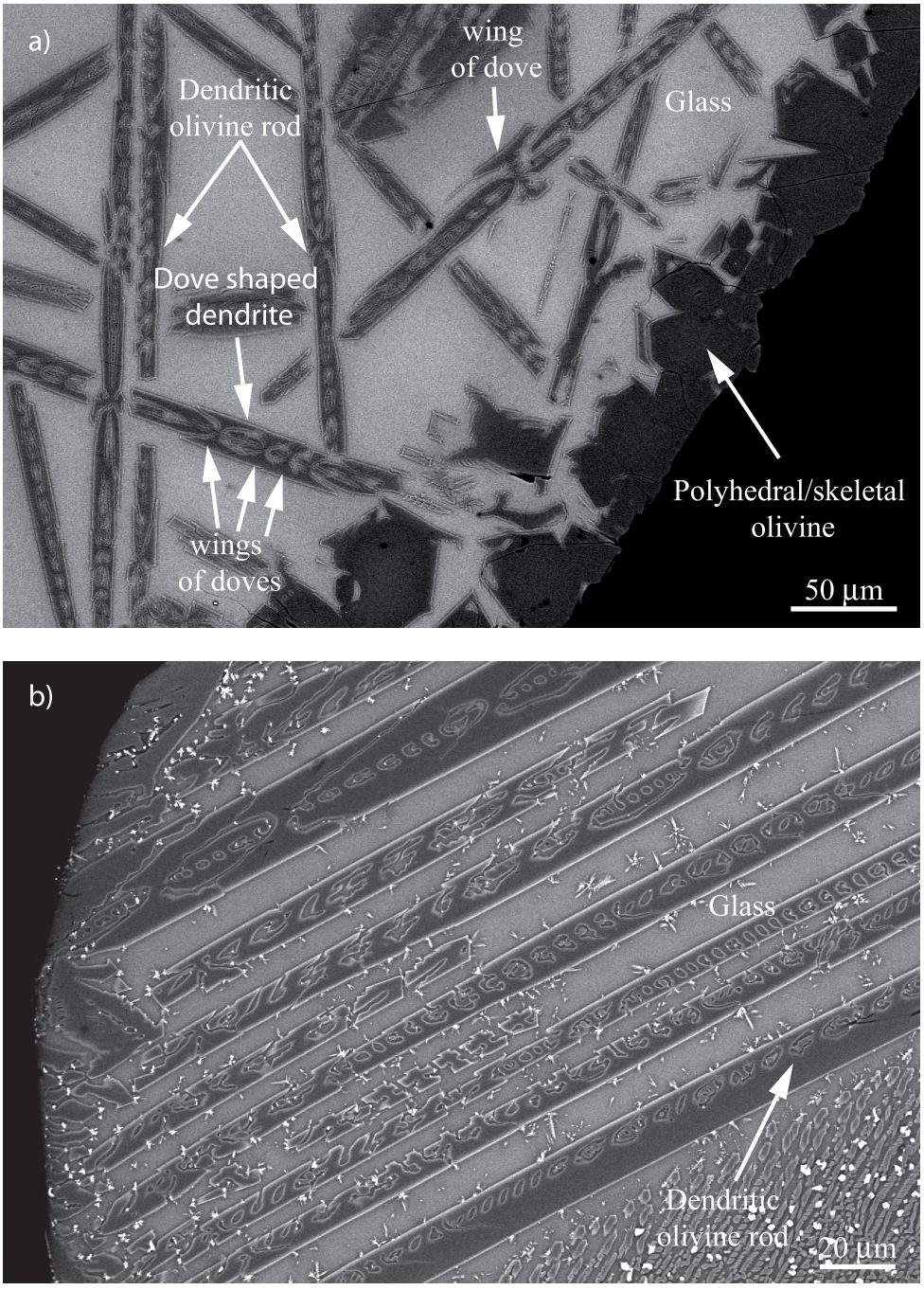

Fig. S1. BSE images of isothermal experimental charges showing dendritic crystal textures produced during air quenching. (a) Experiment 8-N180 was held isothermally at 1450 °C for 16 h before quenching in air and shows both dendritic rods and polyhedral-skeletal olivine crystals. (b) Experiment 7-N173 was held isothermally at 1450 °C for 7 h before quenching in air and shows dendritic parallel rods of olivine..

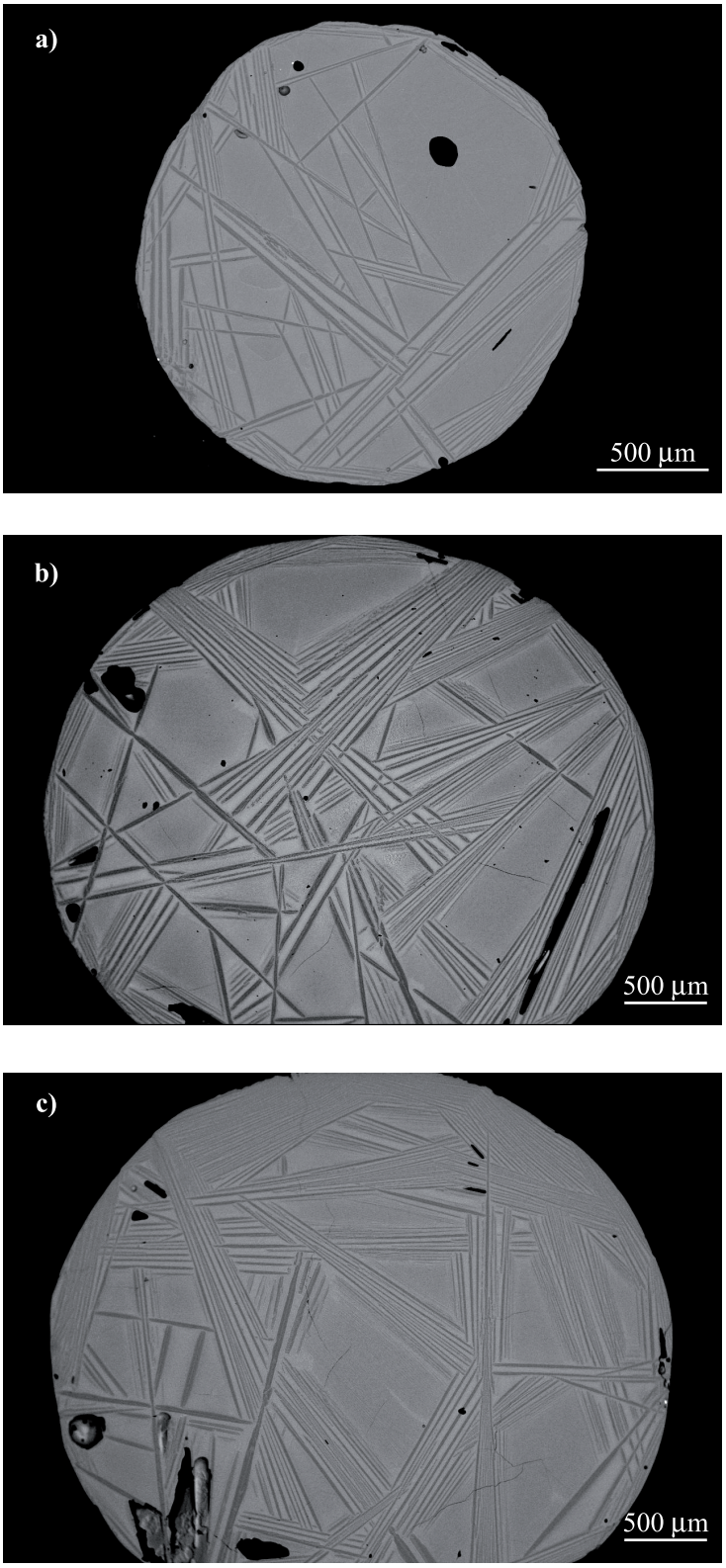

Fig. S2. BSE images of experimental charges showing dendritic crystal textures produced during air quenching. (a) Dynamic crystallisation experiment 40-N269 was cooled to 1200 °C and reheated to 1500 °C; it displays numerous thin dendrites of olivine in the glass mesostasis. (b) Isothermal experiment 12-N194 was held at 1500 °C for 2 h before air quenching and shows a dendritic texture similar to that in (a). (c) Isothermal experiment 16-N234 was held at 1600 °C for 5 minutes before air quenching, and shows a dendritic texture similar to those in (a) and (b).

Table S1. Chemical compositions (EDS analyses, in wt.%) of olivines crystallized during dynamic crystallization experiments.

Run n°	n	SiO_2	Al_2O_3	FeO	MgO	CaO	Fa, mol %
23-N258	4	41.01	0.44	7.75	50.59	0.19	7.85
		(0.12)	(0.08)	(0.30)	(0.28)	(0.01)	(0.32)
24-N259	5	40.94	0.51	7.24	51.04	0.24	7.29
		(0.21)	(0.20)	(0.36)	(0.42)	(0.02)	(0.38)
25-N267	5	41.08	0.53	10.55	47.47	0.34	10.94
		(0.20)	(0.03)	(0.30)	(0.26)	(0.04)	(0.31)
26-N268	4	40.81	0.14	8.09	50.70	0.24	9.94
		(0.13)	(0.09)	(0.23)	(0.21)	(0.04)	(0.29)
27-N260	5	41.46	0.37	9.54	48.31	0.30	9.86
		(0.30)	(0.03)	(0.44)	(0.26)	(0.07)	(0.46)
28-N263	4	41.37	0.27	11.12	46.95	0.26	11.62
		(0.49)	(0.03)	(0.22)	(0.38)	(0.06)	(0.17)
29-N262	4	40.96	0.15	8.65	49.95	0.27	8.78
		(0.14)	(0.12)	(0.59)	(0.47)	(0.07)	(0.61)
30-N299	5	42.71	0.37	5.29	51.37	0.24	5.41
		(0.55)	(0.06)	(0.26)	(0.39)	(0.05)	(0.25)
31-N261	5	42.54	0.21	6.59	50.41	0.23	6.77
		(0.32)	(0.04)	(0.19)	(0.31)	(0.04)	(0.19)
32-N274	4	41.96	0.66	6.63	50.39	0.33	6.78
		(0.34)	(0.02)	(0.20)	(0.29)	(0.05)	(0.19)
33-N273	5	42.41	0.38	6.08	50.86	0.24	6.23
		(0.20)	(0.03)	(0.21)	(0.30)	(0.04)	(0.23)
34-N270	4	42.49	0.07	0.26	56.93	0.22	0.26
		(0.15)	(0.04)	(0.09)	(0.22)	(0.03)	(0.09)
35-N272	6	44.07	0.42	0.03	55.07	0.40	0.03
		(0.47)	(0.10)	(0.04)	(0.41)	(0.04)	(0.04)

Abbreviations: n, number of analyses; Fa, fayalite content

Table S2. Chemical compositions (EDS analyses, in wt.%) and normative mineralogy of glass inclusions in barred olivine chondrules.

sample	A-211	A-212	A-225	A-226	A-228	A-230	A-231	A-232	F-340	S-273	V-1[a]
SiO_2	46.78	51.58	51.02	49.30	48.25	49.16	48.74	51.97	63.90	65.34	47.51
TiO_2	nd	2.46	2.00	2.05	2.74	3.00	3.78	2.43	nd	nd	0.05
Al_2O_3	32.36	19.98	24.77	25.49	21.72	21.18	18.19	20.23	16.13	16.57	32.79
Cr_2O_3	nd	0.93	0.97	1.02	0.82	nd	1.19	1.28	2.15	nd	0.01
FeO	nd	nd	nd	nd	nd	nd	nd	nd	1.16	1.08	0.59
MnO	nd	nd	nd	nd	nd	nd	nd	nd	nd	nd	0.00
MgO	1.45	0.87	1.28	1.04	1.86	1.15	3.85	0.82	3.93	3.98	0.69
CaO	17.38	16.00	8.43	10.34	16.03	18.23	16.59	15.71	4.93	3.20	17.11
Na_2O	2.03	8.17	11.52	10.75	8.57	7.28	7.66	7.56	6.52	8.34	2.07
K_2O	nd	nd	nd	nd	nd	nd	nd	nd	1.29	1.49	0.04
Total	100.00	100.00	100.00	100.00	100.00	100.00	100.00	100.00	100.00	100.00	100.85
An	90.14	61.64	79.06	80.72	67.46	64.40	56.82	62.22	49.51	50.75	91.22
Di	-1.67	21.90	-23.48	-16.50	17.95	28.34	29.08	19.94	-17.11	-25.65	-3.66
Fo	3.12	-5.39	10.25	7.47	-2.14	-6.97	-1.76	-4.87	13.27	16.13	2.41
Qtz	8.41	21.85	34.17	28.31	16.72	14.22	15.86	22.71	54.33	58.76	10.03

Abbreviations: sample A, Allende chondrite; sample F, Felix chondrite; sample S, Sahara chondrite; sample V, Vigarano chondrite; nd, not determined; An, anorthite; Di, diopside; Fo, forsterite; Qtz, quartz.

[a]Analysed by WDS.

Table S3. Chondrule number density and solid:gas ratio as a function of cooling time scale.

T_{in} (K)	T_{end} (K)	Cooling rate (K/h)	Cooling time scale (s)	Collision velocity v (m/s)	Chondrule number density n (m^{-3})	Mass density of precursors ρ_s (Kg/m^3)	Solid:gas density ratio
1900	1400	10	180,000	5	3.55	6.4×10^{-6}	4.5
1900	1200	10	252,000	5	2.53	4.5×10^{-6}	3.2
1800	1400	10	144,000	5	4.44	8.0×10^{-6}	5.7
1800	1200	10	216,000	5	2.96	5.3×10^{-6}	3.8
1900	1400	5	360,000	5	1.77	3.2×10^{-6}	2.2
1900	1200	5	504,000	5	1.26	2.2×10^{-6}	1.6
1800	1400	5	288,000	5	2.22	4.0×10^{-6}	2.8
1800	1200	5	432,000	5	1.48	2.6×10^{-6}	1.9
1900	1400	10	180,000	0.5	35.5	6.4×10^{-5}	45.8
1900	1200	10	252,000	0.5	25.3	4.5×10^{-5}	32.7
1800	1400	10	144,000	0.5	44.4	8.0×10^{-5}	57.2
1800	1200	10	216,000	0.5	29.6	5.3×10^{-5}	38.19
1900	1400	5	360,000	0.5	17.7	3.2×10^{-5}	22.9
1900	1200	5	504,000	0.5	12.6	2.2×10^{-5}	16.3
1800	1400	5	288,000	0.5	22.2	4.0×10^{-5}	28.6
1800	1200	5	432,000	0.5	14.8	2.6×10^{-5}	19.0
Results of Bischoff et al. (2017) calculations							
1900	1400	1,800	1,000	5	640	1.1×10^{-3}	825
1900	1400	18,000	100	5	6,400	1.2×10^{-2}	8,250
1900	1400	1,800	1,000	0.5	6,400	1.2×10^{-2}	8,250
1900	1400	18,000	100	0.5	64,000	1.2×10^{-1}	82,500

T_{in}, initial chondrule temperature; T_{end}, the lowest temperature at which melt could have been present in the chondrule.

n: the local number density of chondrules can be estimated by $n = \frac{0.8}{t_{cool}\, r_p^2\, v}$, where r_p = 0.5 mm is the chondrule radius; v is the collision velocity, which typically varies between 0.5 and 5 m/s; and t_{cool} is the cooling time, which corresponds to the time elapsed before chondrules were too cold to stick together (Bischoff et al., 2017).

ρ_s: the initial local mass density of all chondrule precursor materials can be calculated as $\rho_s = 3.3\, \rho_p\, \frac{r_p}{t_{cool} v}$, where the individual chondrule mass density ρ_s = 3,500 kg/m^3 (Bischoff et al., 2017). The ratio between precursor density and gas density is calculated assuming a mass density of 1.4×10^{-6} kg/m^3 at 1 AU in a minimum-mass solar nebula (Hayashi et al., 1985).